Journal of Engineering Mathematics **24**: 287–310, 1990.

The breakdown of jet flows in a low-Rossby-number rotating fluid

M.A. PAGE and M.D. EABRY
Department of Mathematics, Monash University, Clayton, Victoria 3168, Australia

Received 22 September 1989; accepted 11 December 1989

Abstract. The behaviour of steady jet-like flows is examined in a low-Rossby-number rotating fluid. Unlike the corresponding non-rotating flow, the momentum flux of a jet in a rotating fluid is not conserved with distance downstream and, as a consequence, the jet loses all of its momentum at a finite distance from the source, apparently developing a singularity as this occurs. The asymptotic properties of the flow leading up to this singular point are calculated for jets of various inflow widths and a structure which resolves the singularity that occurs in each of these cases is described. The properties on the approach to the singularity are shown to be similar to those of the exact solution described by Gadgil [12]. Both the asymptotic structure and the resolution of the singularity are, however, applicable to the expected breakdown of any form of jet in rotating fluid under similar conditions. The consequences of this are discussed, particularly in relation to the separated-flow structure proposed for motion past a cylindrical obstacle in Page [3].

1. Introduction

In many ways the behaviour of $E^{1/4}$ layers in a low-Rossby-number rotating-fluid flow reflect the properties of two-dimensional high-Reynolds-number boundary-layer flows. Phenomena such as separation (Walker and Stewartson [1], Page [2, 3]) and wake formation (Page [4]) occur through similar mechanisms to their non-rotating counterparts, although there are some novel effects which arise through the effect of suction from the Ekman layers in these flows, where vortex stretching leads to the removal of vorticitity from the flow. Examples of this are the finite length of the separated region behind a cylindrical object, described in Page [3, 5], and the rapid exponential decay of the vorticity in the wake of an obstacle. These effects have been noted in the experimental results of Boyer [6] and Boyer and Davies [7], and in the numerical calculations by Matsuura and Yamagata [8] and Becker [9].

A further class of boundary-layer flows are narrow jets of fluid moving into an otherwise stagnant fluid, and the archetype of these in a non-rotating fluid is the so-called Bickley jet (Bickley [10], Schlichting [11, p. 172]), where the forcing for the jet is due to a line source of momentum, producing a two-dimensional flow. Despite the apparent idealisation, this describes the far field of a broad class of flows where fluid is injected into a stagnant fluid with a dominant momentum flux in one direction. The corresponding problem in a low-Rossby-number rotating fluid has been considered by Gadgil [12] and it was shown that, apart from close to the source, the jet exhibits rather different properties from those in a non-rotating fluid. The most significant of these is the termination of the jet at a finite distance from the source, forming a singularity as it loses all of its fluid and momentum. To the authors' knowledge, no experimental work has been carried out in precisely this configuration, although the results of a study by Savage and Sobey [13] on a similar flow with a free surface do broadly support Gadgil's conclusions.

In this paper, more general forms of jets, of varying widths and inflow profiles, are examined and it is shown that a similar singularity develops after a finite distance. For jets of small inflow width, in comparison to the $E^{1/4}$-layer thickness, it is shown that the exact solution found by Gadgil [12] is appropriate to leading order. For symmetric jets of width $O(E^{1/4})$ a similar singularity occurs at a distance downstream which is proportional to the maximum velocity in the jet. An asymptotic structure on the approach to this singularity is described, and shown to be identical, to leading order, to that which occurs in Gadgil's exact solution for a small momentum source. The region over which this type of singularity is resolved is then examined and the flow in this region is shown to match smoothly onto the slow secondary motion that is induced by the entrainment and detrainment of the jet. Similar results can be applied to jets wider than $O(E^{1/4})$ at inflow and to those with an asymmetric inflow profile.

Unlike for the rotating flows past obstacles, there is no appropriate zero-Rossby-number form for a jet flow and the governing equations are intrinsically nonlinear in the regime of most interest, when the jet is long compared to its width. For a jet arising from an infinitesimal momentum source, this parameter régime, like considered in Page [4], is such that the flow close to the source is described accurately by the counterpart flow in a non-rotating fluid. In both cases this requires that the Rossby number Ro, based on the imposed momentum flux spread over the width of an $E^{1/4}$ layer, satisfies the restriction $Ro \gg E^{3/4}$, where E is the Ekman number, since for smaller Rossby numbers the momentum introduced by the jet extends no further than a distance of the order of an $E^{1/4}$-layer thickness from the source. A further constraint on the Rossby number for the applicability of the theory is that $Ro \ll E^{1/3}$, in order to ensure, among other things, the validity of the linear analysis used to include the effect of the Ekman layers on the flow.

The plan of the paper is to introduce the governing equations for a jet-type flow in a rotating fluid in Sec. 2, and then apply these to the simplest case of a narrow source in Sec. 3. Symmetric jets with width of $O(E^{1/4})$ are considered in Sec. 4 and the general form of the singularity which occurs for these is described in Sec. 5, followed by the theory for the resolution of this singularity in Sec. 6. The secondary flow which is induced outside of the jet is calculated in Sec. 7. The final case, where the jet is wide compared to the $E^{1/4}$ layer, is described in Sec. 8 and the differences which arise for an asymmetric jet inflow are outlined in Sec. 9. Some consequences of this work are discussed in Sec. 10.

2. Governing equations

Consider a homogeneous incompressible fluid of density ρ^* and constant kinematic viscosity ν^*, contained between two infinite parallel plates, a distance d^* apart, and bounded on one side by another plate extending normally between the two parallel plates, as illustrated in Fig. 1. The entire configuration is rotating with a uniform angular velocity $\Omega^*\mathbf{k}$ about an axis which is perpendicular to the parallel plates so that, relative to the rotating system, both the plates and the fluid are at rest. A jet of fluid of scale width c^* and momentum flux J^* per unit length is then introduced into the otherwise stationary fluid through a slit in the bounding wall which extends in the $\mathbf{k}$ direction, and the flow is permitted to reach steady state. For convenience, the momentum introduced by the source is assumed to be directed normally to the plate along which it lies, although this restriction is not crucial to most of the analysis in this paper.

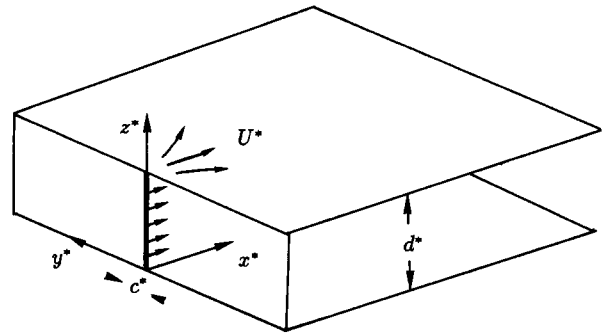

Fig. 1. The flow configuration examined in this paper, relative to a frame rotating about the z^*-axis at an angular velocity Ω^*.

In terms of a velocity scale U^* within the jet it is possible to define Rossby and Ekman numbers for the flow such that

$$Ro = U^*/\Omega^* d^* \quad \text{and} \quad E = \nu^*/\Omega^* d^{*2}\,, \tag{2.1}$$

as in Page [4], and also to introduce dimensionless Cartesian coordinates for the position and velocity given by

$$\mathbf{x} = (x, y, z) = \mathbf{x}^*/d^* \quad \text{and} \quad \mathbf{u} = (u, v, w) = \mathbf{u}^*/U^*\,. \tag{2.2}$$

The origin of these coordinates is chosen as the point of entry of the jet, with the x axis in the direction of the introduced momentum, the y axis extending along the intersection of the plates (as shown in Fig. 1) and z parallel to the rotation axis. As a result, the fluid occupies the region $x>0$ with $-\infty<y<\infty$ and $0<z<1$, and the scale width of the jet in the y direction is equal to $c = c^*/d^*$. In terms of these dimensionless variables the full equation of motion for steady flow is

$$Ro(\mathbf{u}\cdot\nabla)\mathbf{u} + 2(\mathbf{k}\times\mathbf{u}) = -\nabla P + E\nabla^2\mathbf{u}\,, \tag{2.3}$$

where P is the reduced pressure, defined as in Page [4], and $\mathbf{u}$ also satisfies the continuity equation

$$\nabla\cdot\mathbf{u} = 0\,. \tag{2.4}$$

For a low-Rossby-number rapidly-rotating flow, consideration is restricted to the case where $Ro \ll 1$ and $E \ll 1$ so that the momentum equation, to leading order, reduces to the geostrophic constraint

$$2(\mathbf{k}\times\mathbf{u}) = -\nabla P\,. \tag{2.5}$$

It follows immediately from this equation that the dominant part of the motion of the fluid is both depth-independent and two-dimensional, except in thin regions close to solid boundaries. As a result, the velocity components u and v are functions of (x, y) only and the so-called vertical velocity w is zero to leading order. Analysis of the Ekman layers on the

parallel plates (as, for example, in Moore [14]) indicates that there is an $O(E^{1/2})$ vertical flux into and out of these regions, so that w is of order $E^{1/2}$ throughout the interior, and this affects the flow through the next order of approximation to (2.3). Considering these higher-order terms, it turns out that the vertical component of vorticity

$$\zeta = \frac{\partial v}{\partial x} - \frac{\partial u}{\partial y} \tag{2.6}$$

satisfies

$$Ro\left(u\frac{\partial \zeta}{\partial x} + v\frac{\partial \zeta}{\partial y}\right) = (2 + Ro\,\zeta)\frac{\partial w}{\partial z} + E\nabla_h^2 \zeta\,. \tag{2.7}$$

Note that the term $Ro\, w(\partial\zeta/\partial z)$ has been neglected from this equation, in comparison with the other inertial terms since both w and $\partial/\partial z$ are small, and ∇^2 has been replaced by the horizontal Laplacian ∇_h^2. It follows immediately from (2.6) and (2.7) that $\partial w/\partial z$ is independent of z, to an approximation which is accurate to $O(E)$ at least, and using the Ekman compatibility conditions (Moore [14])

$$\frac{\partial w}{\partial z} = -E^{1/2}\zeta \tag{2.8}$$

throughout the depth of the interior flow. At this juncture it is convenient to introduce the two additional parameters

$$\lambda = Ro/2E^{1/2} \quad \text{and} \quad \delta = \left(\frac{1}{2}E^{1/2}\right)^{1/2}, \tag{2.9}$$

as defined in previous low-Rossby-number studies so that, neglecting the relatively-small terms $Ro\,\zeta(\partial w/\partial z)$ in (2.7), the vorticity equation can be written as

$$\lambda\left(u\frac{\partial \zeta}{\partial x} + v\frac{\partial \zeta}{\partial y}\right) = -\zeta + \delta^2\left(\frac{\partial^2 \zeta}{\partial x^2} + \frac{\partial^2 \zeta}{\partial y^2}\right). \tag{2.10}$$

Apart form the scaling parameter λ and the 'Ekman friction' term $-\zeta$, this equation is identical to the vorticity eqation in a non-rotating fluid. Here, δ represents the scale thickness of the viscous shear layers in these flows, known as $E^{1/4}$ layers, and the final term contributes to the leading-order motion only in these regions. Elsewhere (2.10) implies that vorticity is removed from the fluid through the action of the Ekman layers, as for the inviscid flows considered by Page [3].

Since the two-dimensional flow considered in this paper is forced by a narrow momentum source at $x = y = 0$, it can be expected that, as for the corresponding non-rotating flow, motion will be concentrated in a thin jet extending along the x axis. Guided by the scaling in the wake of a flat plate (Page [4]) it is appropriate to introduce the scaled coordinates

$$\bar{x} = x/\lambda \quad \text{and} \quad \bar{y} = y/\delta\,, \tag{2.11}$$

along with a scaled width $\bar{c} = c/\delta$ of the jet and the velocity components

$$\bar{u} = u \quad \text{and} \quad \bar{v} = \lambda v/\delta\,. \tag{2.12}$$

Neglecting terms of relative magnitude $O(\delta^2)$, (2.14) then becomes

$$\bar{u}\frac{\partial\bar{\zeta}}{\partial\bar{x}}+\bar{v}\frac{\partial\bar{\zeta}}{\partial\bar{y}}=-\bar{\zeta}+\frac{\partial^2\bar{\zeta}}{\partial\bar{y}^2}\,, \tag{2.13}$$

where, as for most boundary-layer flows, $\bar{\zeta}=-\partial\bar{u}/\partial\bar{y}$ to within a similar accuracy. Integrating this equation once with respect to $\bar{y}$, using that the flow is stagnant with $\bar{u}\to 0$ at the outer edge of the jet, yields the boundary-layer-type equation

$$\bar{u}\frac{\partial\bar{u}}{\partial\bar{x}}+\bar{v}\frac{\partial\bar{u}}{\partial\bar{y}}=-\bar{u}+\frac{\partial^2\bar{u}}{\partial\bar{y}^2}\,, \tag{2.14}$$

which should be solved in conjunction with the continuity equation

$$\frac{\partial\bar{u}}{\partial\bar{x}}+\frac{\partial\bar{v}}{\partial\bar{y}}=0\,. \tag{2.15}$$

This pair of equations governs the flows considered in most of the remainder of this paper, subject to the specification of a velocity profile $\bar{u}_0(\bar{y})$ at the 'initial' point $\bar{x}=0$.

Before proceeding, it is useful to unravel the coordinate changes in the above analysis and reconsider the flow in dimensional terms. First, the scale thickness of the $E^{1/4}$ layer is δd^*, or

$$\delta^*=\left(\frac{\nu^* d^{*2}}{4\Omega^*}\right)^{1/4} \tag{2.16}$$

in terms of the original parameters. Secondly, the length scale of the jet is λd^*, or

$$l^*=\frac{U^* d^*}{2(\Omega^*\nu^*)^{1/2}} \tag{2.17}$$

in terms of the velocity scale U^*. To calculate this velocity scale for a given 'initial' profile with a specified momentum flux

$$J^*=\int_{-\infty}^{\infty}\rho^* u^{*2}\,\mathrm{d}y^* \quad \text{at} \quad x^*=0 \tag{2.18}$$

we note that over a layer of thickness $O(\delta^*)$, the velocity has magnitude

$$U^*=\left(\frac{J^*}{\rho^*\delta^*}\right)^{1/2}. \tag{2.19}$$

This can then be substituted into (2.1) to determine the appropriate value or Ro, and hence λ for that flow. It is then a simple matter to evaluate the magnitude of J^* for which the low-Rossby-number flow constraints $E^{3/4}\ll Ro\ll E^{1/3}$, described in Sec. 1, are satisfied.

As a direct consequence of the scaling (2.19), the appropriate initial condition for the flows considered here is that the normalised momentum flux

$$\bar{J}(\bar{x})=\int_{-\infty}^{\infty}\bar{u}(\bar{x},\bar{y})^2\,\mathrm{d}\bar{y} \tag{2.20}$$

is equal to unity at $\bar{x} = 0$. For cases where the velocity scale U^* is imposed through other means, so that $\bar{J}$ is not necessarily equal one at $\bar{x} = 0$, the analysis in this paper remains valid subject to the minor rescaling described in Sec. 10.

3. The case $\bar{c} \ll 1$

When the width of the jet is much smaller than $E^{1/4}$, the motion close to the inflow behaves similarly to that in the equivalent problem in a nonrotating fluid, since the 'Ekman suction' term $-\bar{u}$ in (2.14) remains small for $\bar{x} \ll 1$ compared to the other terms in that equation (each of which involve spatial derivatives). As a result, the flow evolves over a short lengthscale of order $\bar{c}$ into the same 'sech^2' velocity profile that would occur for a two-dimensional point source of momentum of that strength (as described, for example, in Schlichting [11]). The resulting jet introduces only a small $O(\bar{c}^{1/2})$ flux of fluid through the inflow but the motion produced by the momentum source induces an O(1) scaled mass flux, fed from the surrounding fluid, which spreads out over a lateral distance of order $\bar{x}^{2/3}$ and contains velocities of $O(\bar{x}^{-1/3})$ while $\bar{c} \ll \bar{x} \ll 1$.

The subsequent motion of a jet of this form was examined by Gadgil [12], who showed that the flow retains a characteristic sech^2 velocity profile for $\bar{x}$ of O(1) with an exact solution to (2.14) of the form

$$\bar{\psi} = -F(\bar{x}) \tanh[\bar{y}G(\bar{x})] , \tag{3.1}$$

in terms of a stream function $\bar{\psi}$ defined in the usual way through

$$\bar{u} = -\frac{\partial \bar{\psi}}{\partial \bar{y}} \quad \text{and} \quad \bar{v} = \frac{\partial \bar{\psi}}{\partial \bar{x}} . \tag{3.2}$$

Substituting (3.1) into (2.14) yields a pair of ordinary differential equations for the two functions F and G, which can be easily solved to yield that

$$F(\bar{x}) = 6(\bar{x} + B)G(\bar{x}) \quad \text{and} \quad G(\bar{x}) = \left[\frac{A(\bar{x} + B)^{-4/3} - 1}{8} \right]^{1/2} , \tag{3.3}$$

in terms of two arbitrary constants A and B. It is then straightforward to show that the appropriate values of these constants for an effective point source of unit momentum flux at $\bar{x} = 0$ are $A = (2/9)^{1/3}$ and $B = 0$, a solution which was originally derived in a magneto-hydrodynamic context by Moreau [15]. Since G decreases monotonically as $\bar{x}$ increases, and eventually equals zero, Moreau noted that the flow develops a singularity once the jet has moved only a finite distance from its source, at $\bar{x}_s = (2/9)^{1/4}$ with the normalisation here. At this point both the momentum and mass fluxes of the jet are equal to zero and the motion due to the source can extend no further into the fluid. To examine the development of the flow leading up to this singularity, several important properties of the jet described by the exact solution (3.1) are shown on Fig. 2 as functions of the distance $\bar{x}$ from the source. Notable on Fig. 2(a) is that the centerline velocity $\bar{u}(\bar{x}, 0)$ decreases rapidly from its large value when $\bar{x} \ll 1$ to approach zero as $\bar{x} \to \bar{x}_s$. Detailed examination of this curve shows that its slope tends towards negative one in this limit, suggesting that the viscous term $\partial^2 \bar{u}/\partial \bar{y}^2$ is relatively small on the centerline on the approach to the singularity. Also apparent from the

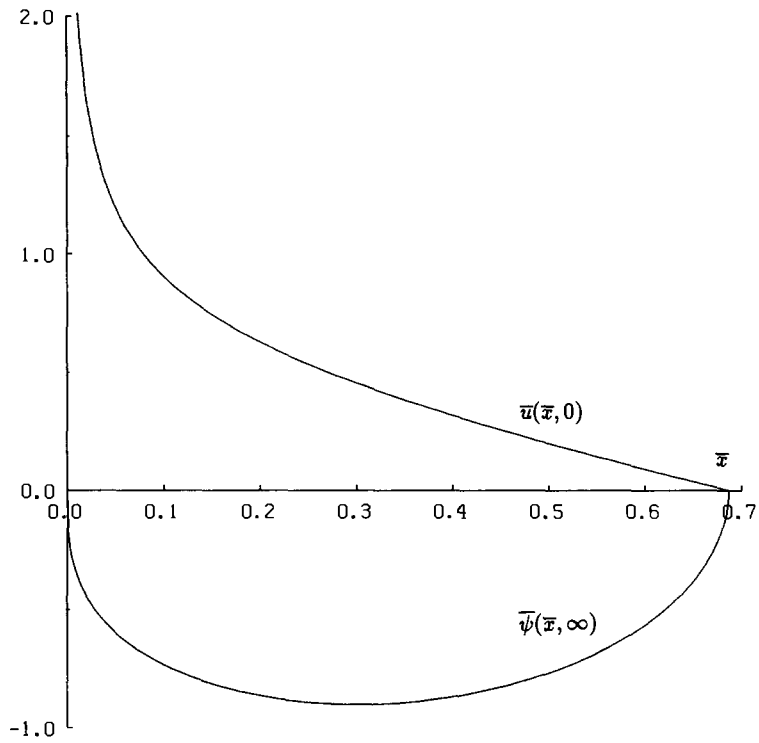

(a)

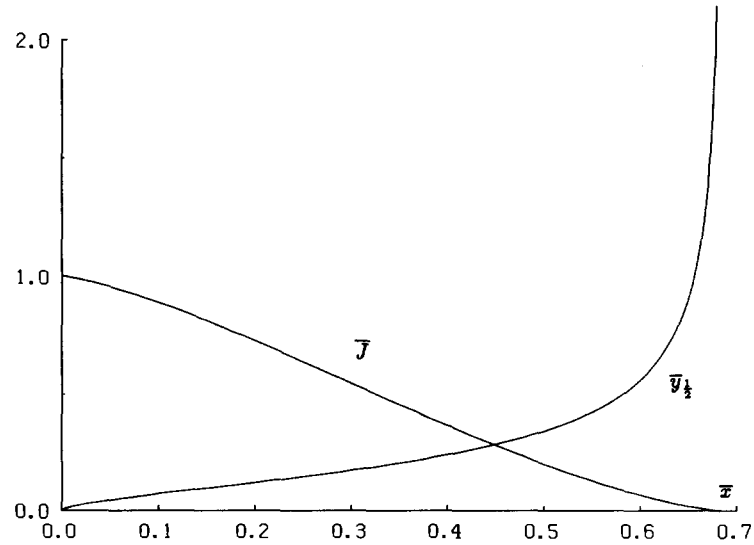

(b)

Fig. 2. Plots of (a) $\bar{\psi}_\infty(\bar{x})$ and $\bar{u}(\bar{x},0)$, and (b) $\frac{1}{10}\bar{y}_{1/2}$ (defined in the text) and $\bar{J}$, as functions of the distance $\bar{x}$ along a jet due to a momentum source.

values of $\bar{\psi}_\infty(\bar{x}) = \bar{\psi}(\bar{x}, \infty)$ in Fig. 2(a) is that the jet entrains fluid initially but that once $\bar{x}$ is larger than about 0.301 it begins to expell the same fluid at its outer edge, so that it has been emptied by the point $\bar{x} = \bar{x}_s$. In particular, the slope of $\bar{\psi}_\infty(\bar{x})$ becomes unbounded as $\bar{x} \to \bar{x}_s$, indicating that the 'blowing velocity' at the outer edge of the jet, $\bar{v}_\infty = \mathrm{d}\bar{\psi}_\infty/\mathrm{d}\bar{x}$, increases indefinitely on the approach to this point. As this occurs the jet thickens rapidly, as is indicated by the values of $\bar{y}_{1/2}$ on Fig. 2(b), defined as the positions where the velocity of the jet is equal to half of its centerline value. Also shown on Fig. 2(b) is the momentum flux $\bar{J}(\bar{x})$ which has unit value at $\bar{x} = 0$ and approaches zero as $\bar{x} \to \bar{x}_s$. As noted by Gadgil [12] (and Moffatt and Toomre [16] in the MHD context) this satisfies the relation

$$\frac{\mathrm{d}\bar{J}}{\mathrm{d}\bar{x}} = 2\bar{\psi}_\infty(\bar{x}) , \tag{3.4}$$

so that it decreases monotonically while the jet contains fluid but decreases more slowly on the approach to the singularity. In contrast, the momentum flux of any jet in a nonrotating fluid is conserved.

One advantage of the exact solution (3.1) for flows with $\bar{c} \ll 1$ is that the structure of the flow on the approach to the singularity is readily calculable. In particular, it can be shown that both F and G are proportional to $(\bar{x}_s - \bar{x})^{1/2}$ as $\bar{x} \to \bar{x}_s$ and hence that $\bar{\psi}_\infty$ decreases in the same manner. In addition, both the blowing velocity $\bar{v}_\infty$ and the thickness $\bar{y}_{1/2}$ are proportional to $(\bar{x}_s - \bar{x})^{-1/2}$, while the centreline velocity approaches $(\bar{x}_s - \bar{x})$. It will be seen in Sec. 5 that all of these properties are more generally applicable to any narrow jet flow in a low-Rossby-number rotating fluid.

4. The case $\bar{c} = \mathrm{O}(1)$

Once the width of the jet at inflow is of the same magnitude as $E^{1/4}$, the full equation (2.14) governs the flow for all $\bar{x} > 0$, and the precise form of the initial profile $\bar{u}_0(\bar{y})$ will affect the development of the jet for $\bar{x}$ of O(1). No exact solution of (2.14) is available in this general case and so to examine this development it is necessary to use a numerical approach. Before pursuing this, however, a number of general results can be outlined which suggest that a singularity will also develop at a finite value of $\bar{x}$ in this case.

First, as pointed out in Sec. 3, the momentum flux of any jet will satisfy (3.3) and $\bar{J}$ will decrease monotonically as the jet proceeds. This alone does not immediately imply that $\bar{J}$ and $\bar{\psi}_\infty$ will equal zero after a finite distance $\bar{x}$, but it does indicate that $\bar{\psi}_\infty$ must eventually become an increasing function of $\bar{x}$. Also, since a jet with $\bar{u} \geqslant 0$ cannot transport mass without momentum (or vice versa), then should $\bar{J}$ and $\bar{\psi}_\infty$ ever vanish they must both do so at the same point $\bar{x}_s$, in which case $\mathrm{d}\bar{J}/\mathrm{d}\bar{x}$ will also equal zero.

Consideration of the momentum equation (2.14), evaluated for each $\bar{x}$ at the point $\bar{y}$ where the jet has its maximum velocity, suggests that a finite point $\bar{x}_s$ will exist; if $\bar{u}$ is the velocity at this maximum then it satisfies the equation

$$\bar{u}\frac{\partial \bar{u}}{\partial \bar{x}} = -\bar{u} + \frac{\partial^2 \bar{u}}{\partial \bar{y}^2} , \tag{4.1}$$

with $\partial^2\bar{u}/\partial\bar{y}^2 \leqslant 0$, and therefore the value of $\partial\bar{u}/\partial\bar{x}$ along that line is at most negative one. For a symmetric jet with a single maximum at $\bar{y} = 0$, this implies that $\bar{u}$ must cross zero

before the point $\bar{x} = \bar{u}_0(0)$ and therefore that $\bar{x}_s \leqslant \bar{u}_0(0)$. Furthermore, since diffusion will act to decrease the value of $|\partial^2\bar{u}/\partial\bar{y}^2|$ on the centreline as the jet proceeds, $\bar{u}$ will remain positive at least until the smaller value $\bar{x} = \bar{u}_0(0)^2/(\bar{u}_0(0) - \bar{u}_0''(0))$.

The behaviour of the flow at the outer edge for $\bar{y} \gg 1$ can also provide some information about the thickening of the jet since the velocity $\bar{u}$ in that vicinity satisfies (Gadgil [12])

$$\bar{v}_\infty \frac{\partial\bar{u}}{\partial\bar{y}} = -\bar{u} + \frac{\partial^2\bar{u}}{\partial\bar{y}^2}\,, \tag{4.2}$$

where $\bar{v}_\infty$ is the blowing velocity defined earlier. As a result, $\bar{u}$ decays exponentially to zero is proportion to $e^{-\gamma\bar{y}}$, where $\gamma = \frac{1}{2}[-\bar{v}_\infty + \sqrt{\bar{v}_\infty^2 + 4}]$. While $\bar{v}_\infty$ is negative, and the jet is importing fluid, this decays faster than $e^{-\bar{y}}$ but once $\bar{v}_\infty$ becomes positive the rate of decay decreases, suggesting that the jet is widening. The extreme case of this occurs as $\bar{v}_\infty$ becomes large and $\gamma \sim 1/\bar{v}_\infty$, implying that the scale thickness of the jet is equal to $\bar{v}_\infty$ in this situation; the flow at the outer edge of the jet is then predominantly inviscid.

To examine the precise behaviour of jets of width $O(E^{1/4})$, several different initial profiles were chosen. The simplest case is when the inflow has a sech^2 profile, since then the exact solution (3.1) can be used to determine the relevant flow quantities. Choosing

$$\bar{u}_0(\bar{y}) = \left(\frac{3}{4\bar{c}}\right)^{1/2} \mathrm{sech}^2(\bar{y}/\bar{c})\,, \tag{4.3}$$

(in accordance with the normalisation in Sec. 2) it can easily be shown that the appropriate values of the constants in (3.3) are $A = (8/\bar{c}^2 + 1)B^{4/3}$ and $B = \frac{1}{4}\sqrt{\bar{c}^3/3}$, and these can be used to plot similar quantities to those examined for the jet due to a point source in Sec. 3. In particular, the values of both the centreline velocity and $\bar{\psi}_\infty$ are shown on Fig. 3 for several values of $\bar{c}$, and it is clear from these that a singularity develops in each case, at a point which moves closer to $\bar{x} = 0$ as $\bar{c}$ increases. For $\bar{c} < 1$ the jet enters the flow with a finite mass flux and then entrains fluid before beginning to detrain once $G(\bar{x})$ falls below $\frac{1}{2}$, with the mass flux falling to zero as G vanishes. This is similar to the behaviour seen in Sec. 3. For $\bar{c} > 1$ the jet detrains fluid as soon as it enters the flow with $\bar{\psi}_\infty$ approaching zero more rapidly as $\bar{c}$ is increased. In all cases the centreline velocity decreases to zero with the same slope $\partial\bar{u}/\partial\bar{x}$ as $\bar{x} \to \bar{x}_s$ and for the larger values of $\bar{c}$ this slope is almost constant for all $\bar{x}$.

The development of a sech^2 initial profile need not, however, be typical since the velocity profile remains the same shape for all stations $\bar{x}$. To examine the development of other forms of jet, several different inflow profiles were chosen and (2.14) was integrated numerically using the box method (Keller and Cebeci [17]). In these computations up to 100 gridpoints were used in both the $\bar{x}$ and $\bar{y}$ directions, with a geometric stretching in $\bar{y}$ extending out to $\bar{y}_\infty = 25$. In expectation of the thickening of the jet, a modified boundary condition was used at $\bar{y}_\infty$ which ensured that $(\bar{v}\,\partial\bar{u}/\partial\bar{y} + \bar{u})$, rather than $\bar{u}$, was zero at the outer edge of the computational domain. This can be justified from the asymptotic behaviour expected from (4.2) for $\bar{v}_\infty \gg 1$, but it does not alter the profiles unless the thickness of the jet is of the same magnitude as $\bar{y}_\infty$.

In principle, any initial profile with $\bar{u}_0$ positive everywhere can be specified but, for simplicity, consideration here is restricted to symmetric jets with a single velocity maximum. Discussion of asymmetric jets is deferred until Sec. 9. The profiles chosen for presentation here are:

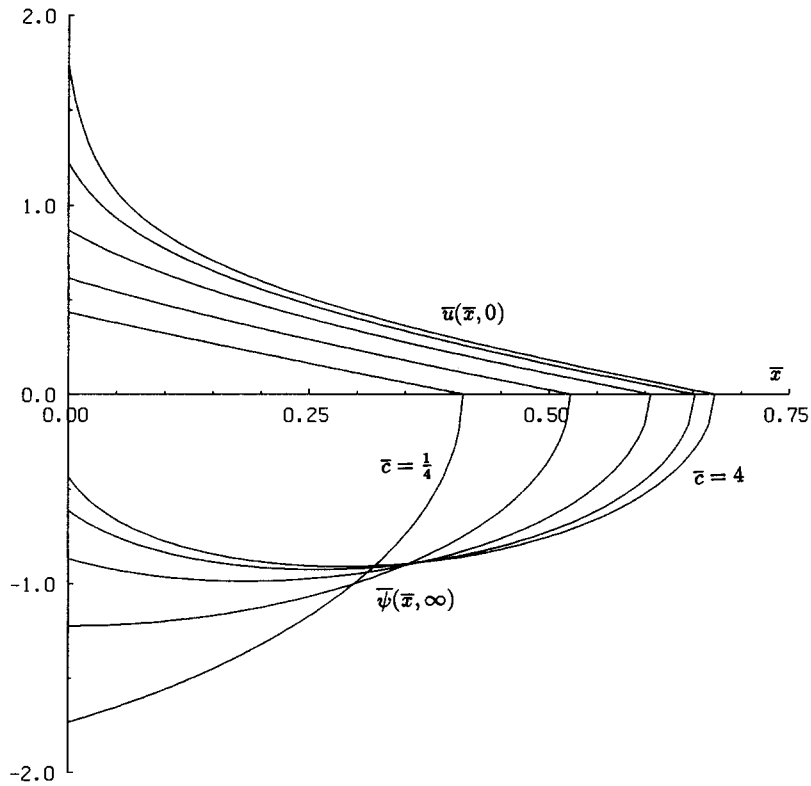

Fig. 3. Plots of $\bar{\psi}_\infty(\bar{x})$ and $\bar{u}(\bar{x},0)$ for the inflow profile (4.3) with $\bar{c}=\frac{1}{4}, \frac{1}{2}, 1, 2, 4$.

$$\begin{aligned}
&\text{(a)}\quad \bar{u}_0(\bar{y}) = \alpha \exp(-\bar{y}^2/\bar{c}^2)\,,\\
&\text{(b)}\quad \bar{u}_0(\bar{y}) = \alpha/(\bar{y}^2+\bar{c}^2)\,,\\
&\text{(c)}\quad \bar{u}_0(\bar{y}) = \alpha\{\tanh[10(\bar{y}/\bar{c}+1)] - \tanh[10(\bar{y}/\bar{c}-1)]\}\,,
\end{aligned} \tag{4.4}$$

where in each case α is calculated to ensure that $\bar{J}_0 = 1$. Note that the first two of these profiles do not decay exponentially at their outer edge, in the form predicted from (4.2), and therefore $\bar{v}_\infty$ is not finite at $\bar{x}=0$ (this did not, however, appear to affect the development of the singularity which is more dependent on the behaviour of the flow for $\bar{\psi} \ll 1$). The results of the numerical calculations for each of these profiles are summarised on Fig. 4, where the values of $\bar{u}(\bar{x},0)$ and $\bar{\psi}_\infty$ are shown for one choice of $\bar{c}$. In all cases $\bar{u}(\bar{x},0)$ tends to zero with a slope of negative one and the jet empties at the same point while $\bar{v}_\infty$ becomes unbounded. In the vicinity of the singularity the form of the solution in each case appears to be identical to those shown in Figs 2 and 3. Plots of $\bar{J}$ and $\bar{y}_{1/2}$ (not shown here) also show a similar behaviour to those for the sech^2 profiles (4.3), with the jet thickening as it loses momentum. To illustrate the form of the flow in this limit, some velocity profiles corresponding to profile (4.4c) are shown in Fig. 5 at various values of $\bar{x}$. This profile was chosen to have similar a 'top hat' shape for $\bar{x}=0$ but the velocities spread out rapidly as $\bar{x}$ is increased, forming into a diffuse profile with a shape rather like sech^2 on the approach to $\bar{x}_s \approx 0.5$.

While the results of the numerical calculations presented here cannot be considered conclusive proof, they do, along with the general properties outlined at the start of this

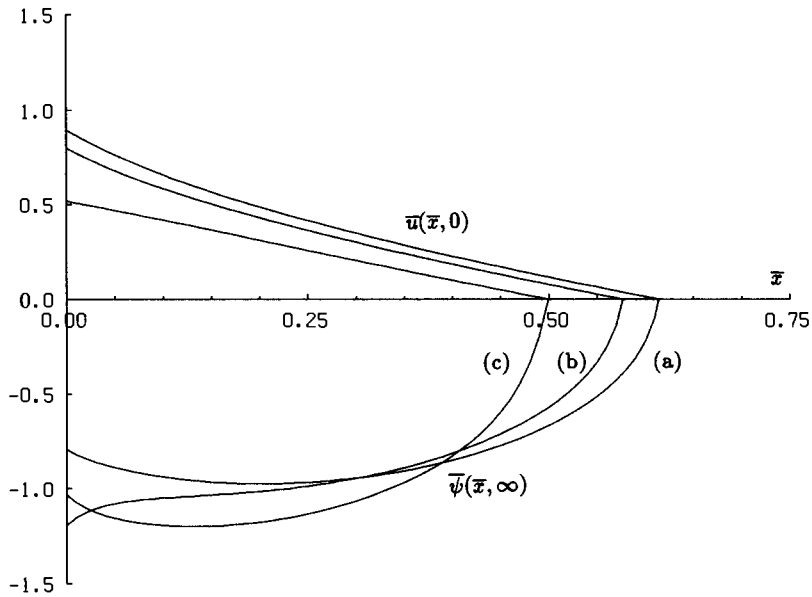

Fig. 4. Plots of $\bar{\psi}_\infty(\bar{x})$ and $\bar{u}(\bar{x},0)$ for each of the inflow profiles (4.4) with $\bar{c}=1$ for (a), (b) and $\bar{c}=2$ for (c).

section, strongly support the assertion that any form of jet will break down in a singular region after proceeding only a finite distance into the fluid. For a fixed value of the momentum flux this distance appears to decrease as the width of the jet increases (due to the corresponding decrease in the centreline velocity at $\bar{x}=0$), and the blowing velocities at the outer edge of the jet become stronger on the approach to the singularity as $\bar{c}$ is increased. The resemblance in form of the numerical solutions in Figs 2, 3 and 4 on the approach to the singularity suggest that this singularity has a generic form for all types of jets. This is supported by the form of the velocity profiles as $\bar{x}\to\bar{x}_s$ in Fig. 5 and is pursued in the following section.

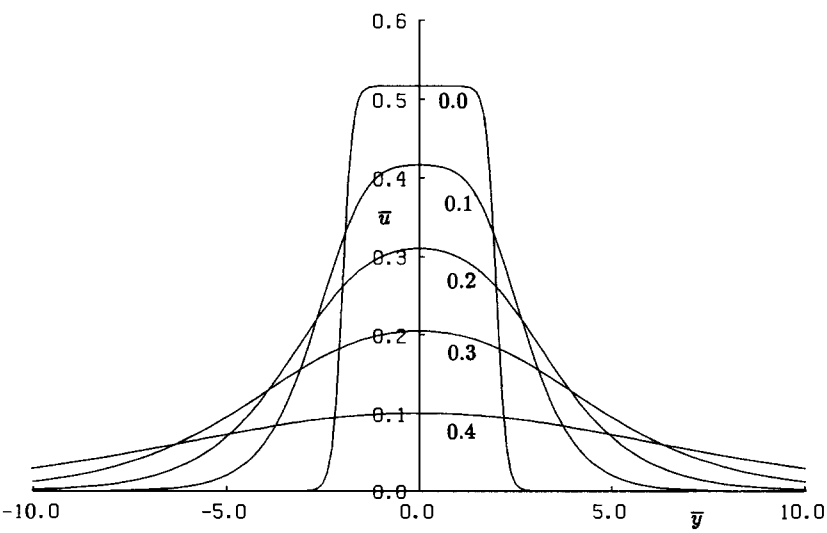

Fig. 5. Plots of the velocity profiles $\bar{u}(\bar{x},\bar{y})$ based on numerical calculations with the initial profile (4.4c) with $\bar{c}=2$, plotted at $\bar{x}=0.0$, 0.1, 0.2, 0.3, 0.4.

5. Approach to the singularity

Some of the features of the numerical solutions described in Sec. 4 suggest that an analytical structure for the approach to the singularity at $\bar{x} = \bar{x}_s$ may be obtainable for any form of inflow profile, much as it is available from the exact solution in Sec. 3 for sech^2 profiles. In particular, the decrease in the velocities in the jet in proportion to $(\bar{x}_s - \bar{x})$ and the increase in the thickness of the layer are reminiscent of features of the flow near the rear stagnation point of a circular cylinder, described in Page [18] and Page and Cowley [19], suggesting that the flow in the vicinity of $\bar{x}_s$ may be predominantly inviscid. As a result, a similar technique to that used in Page and Cowley [19] is used again here, transforming the inviscid form of (2.14) into Von Mises coordinates $(\bar{x}, \bar{\psi})$ so that the flow near $\bar{x}_s$ satisfies

$$\bar{u} \frac{\partial \bar{u}}{\partial \bar{x}} = -\bar{u} \,. \tag{5.1}$$

This equation can be integrated with respect to $\bar{x}$ to yield the explicit solution

$$\bar{u} = (\bar{x}_s - \bar{x}) - h(\bar{\psi}) \tag{5.2}$$

in terms of an unknown function h which, as in Page and Cowley, should be calculable from the flow upstream of the singularity. The solution (5.2) is similar to equation (6.1) in Gadgil [12], but the key to determining $h(\bar{\psi})$ in this context is the recognition that (5.2) remains valid everywhere in the region for which $\bar{\psi} \ll 1$, and this is not only near $\bar{x} = \bar{x}_s$ but also near $\bar{y} = 0$ for $\bar{x} < \bar{x}_s$. For the symmetry of $\bar{u}$ and the influence of diffusive effects across $\bar{y} = 0$ the form of $\bar{u}$ for $\bar{y} \ll 1$ is

$$\bar{u} \sim (\bar{x}_s - \bar{x}) - \mathrm{O}(\bar{y})^2 \tag{5.3}$$

and using also that $\bar{\psi} \sim (\bar{x} - \bar{x}_s)\bar{y}$ in the same region implies that h is proportional to $\bar{\psi}^2$ for $\bar{\psi}$ small. It follows immediately from the form of (5.3) that the equation for $\bar{u}$ sufficiently close to the singularity can be written as

$$\bar{u} = (\bar{x}_s - \bar{x}) - a^2 \bar{\psi}^2 \,, \tag{5.4}$$

for some constant a, chosen to be non-negative. As a consequence, near the outer edge of the jet where $\bar{u} = 0$ and $\bar{\psi} = \bar{\psi}_\infty$, the streamfunction must satisfy

$$0 = (\bar{x}_s - \bar{x}) - a^2 \bar{\psi}_\infty^2 \,, \tag{5.5}$$

and hence

$$\bar{\psi}_\infty(\bar{x}) \sim -(\bar{x}_s - \bar{x})^{1/2}/a \tag{5.6}$$

as $\bar{x} \to \bar{x}_s$. This demonstrates that, in the general case, $\bar{\psi}_\infty$ behaves algebraically in a similar manner to the exact solution in Sec. 3, with the thickness of the layer also increasing in proportion to $(\bar{x}_s - \bar{x})^{-1/2}$ in the same limit.

To obtain more details of this structure, (5.4) can be written in terms of the original coordinates $(\bar{x}, \bar{y})$ in the form

$$-\frac{\partial \bar{\psi}}{\partial \bar{y}} = (\bar{x}_s - \bar{x}) - a^2 \bar{\psi}^2 \tag{5.7}$$

and integrated with respect to $\bar{y}$ to yield the solution

$$\bar{\psi} = -(\bar{x}_s - \bar{x})^{1/2} \tanh[a\bar{y}(\bar{x}_s - \bar{x})^{1/2}]/a\,, \tag{5.8}$$

equivalent to that described for a 'bottom frictional jet' in Gadgil [12]. The corresponding velocity profile can then be calculated as

$$\bar{u} = (\bar{x}_s - \bar{x}) \operatorname{sech}^2[a\bar{y}(\bar{x}_s - \bar{x})^{1/2}]\,, \tag{5.9}$$

and this matches closely with the numerical solutions in Fig. 5 close to the singularity. The reoccurrence of the sech^2 velocity profile, like that in the exact solution, is remarkable. To determine completely the solution in (5.8) and (5.9), the appropriate value of the parameter a for any particular initial condition needs to be evaluated, and this can be obtained from the numerical solutions close to $\bar{x} = \bar{x}_s$. This was achieved by evaluating $\partial^2 \bar{u}/\partial \bar{y}^2$ on $\bar{y} = 0$ and using these as $\bar{x} \to \bar{x}_s$ to deduce the value of a that matches with (5.4) in each case. Some care was necessary in this procedure since the numerical method used in Sec. 4 is only second-order accurate and the truncation errors in the calculations are of the same magnitude as the values of $\partial^2 \bar{u}/\partial \bar{y}^2$ near $\bar{x}_s$; to minimise these errors, Richardson extrapolation was used at fixed values of $\bar{x}$, before dividing by $(\bar{x}_s - \bar{x})^2$ to yield $-2a^2$. Despite these difficulties, the values of a listed in Table 1, obtained using extrapolation on profiles with up to 100 points in both $\bar{x}$ and $\bar{y}$, were consistent to 2 significant figures. In particular, since the exact solution corresponding to profile (4.3) is known exactly, it can be shown that $a = (8 + \bar{c}^2)^{-3/4}/\sqrt{2}$ and hence that the value given for this profile is accurate to 2 decimal places; this suggests that the other values in Table 1, obtained using a similar method, are likely to be equally accurate.

Table 1. Singularity positions $\bar{x}_s$ and values of the parameter a in (5.8) for each of the profiles in (4.4) and (4.5) using the stated values of $\bar{c}$

Profile	$\bar{c}$	$\bar{x}_s$	a
(4.4a)	1	0.605	0.470
(4.4b)	1	0.614	0.481
(4.4c)	1	0.577	0.471
(4.5)	2	0.500	0.340

The solution outlined above identifies the precise nature of the singularity as any form of jet empties, with the $\bar{u}$ velocity component changing abruptly from a linear decrease for $\bar{x} < \bar{x}_s$ to a completely stagnant flow with $\bar{u} = 0$ once $\bar{x} > \bar{x}_s$. This behaviour is clear in Fig. 6, where the streamlines based on (5.8) are shown, and there is no apparent connection between the flow on either side of $\bar{x} = \bar{x}_s$ (identified by the broken line). Perhaps more noticeable is that the blowing velocity $\bar{v}_\infty$ at the outer edge of the jet, from (5.6), is

$$\bar{v}_\infty \sim (\bar{x}_s - \bar{x})^{-1/2}/2a \tag{5.10}$$

for $\bar{x} < \bar{x}_s$ but zero for $\bar{x} > \bar{x}_s$. This opens the question of how such a marked change in behaviour across $\bar{x} = \bar{x}_s$ can be resolved and why the boundary-layer equations develop a singularity at that point. This is pursued in the following section.

Finally, although the solution (5.8) was derived here using a transformation into Von Mises coordinates, a more traditional similarity approach, assuming that

$$\bar{\psi} = (\bar{x}_s - \bar{x})^{\alpha} f(\bar{y}(\bar{x}_s - \bar{x})^{\beta})\,, \tag{5.11}$$

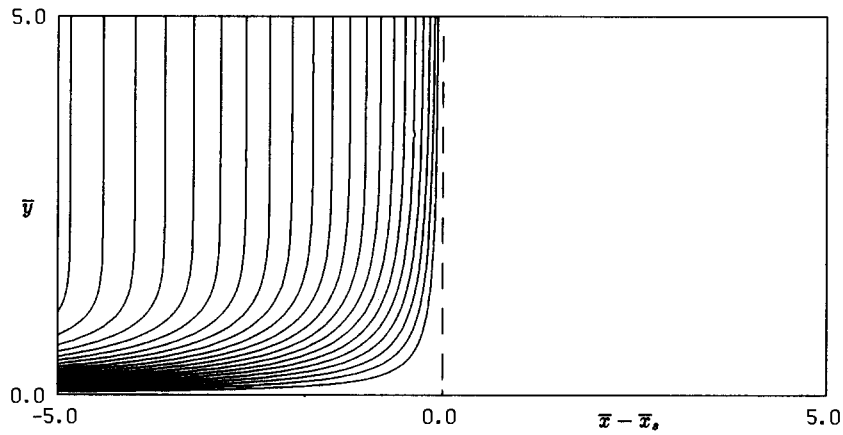

Fig. 6. Streamlines of the flow on the approach to the singularity, based on the analytical solution (5.8) with $a = 1$. The flow is plotted over the region $-5 \leqslant \bar{x} - \bar{x}_s \leqslant 5$ and $0 \leqslant \bar{y} \leqslant 5$ with contour interval $\Delta\bar{\psi} = 0.1$.

for constants α and β, yields an identical solution. This was the method used in Sec. 4.2 of Gadgil [12] to solve an equivalent equation to (5.1). However, since no matching was performed with the $\bar{y} \ll 1$ flow in that paper, the result that $\alpha = \frac{1}{2}$, obtained here, was not available. In general, the technique of using $\bar{\psi}$ rather than $\bar{y}$ as an independent variable is preferable to assuming a solution of the form (5.11) since no *a priori* assumptions about the algebraic behaviour of both $\bar{\psi}$ and the thickness of the layer are necessary.

6. Resolution of the singularity

The structure of the flow on the approach to the singular point $\bar{x} = \bar{x}_s$ outlined for $\bar{c} \ll 1$ and $\bar{c} = O(1)$ in Sec. 3 and Sec. 5, particularly the development of the blowing velocity $\bar{v}$ in (5.10), suggests that some of the $\bar{x}$ derivatives neglected in the formulation of (2.14) will eventually become important. Further, with the thickening of the layer as $\bar{x} \to \bar{x}_s$ there will eventually be a point where the jet can no longer be considered to be relatively thin and therefore a rescaling of the full equations (2.6) and (2.10) appears to be necessary near $\bar{x}_s$. Moffatt and Toomre [16] considered a similar rescaling in the magnetohydrodynamic context but, since behaviour of the flow outside of the jet is very different in that case, their results are not immediately applicable here (nor, as it turns out, are they quite so simple).

Comparing the sizes of the two terms on the right-hand side of (2.6), it is clear that the $\partial v/\partial x$ term is going to increase as the singularity is approached while the $\partial u/\partial y$ term, considered to be dominant in boundary-layer analysis, is going to decrease as the layer thickens and u approaches zero. Using the sizes of these terms based on the solution presented in Sec. 5, it is clear that they will be of the same magnitude once

$$\frac{\delta}{a\lambda^{1/2}(x_s - x)^{3/2}} \sim \frac{a(x_s - x)^{3/2}}{\delta\lambda^{3/2}} \tag{6.1}$$

and this suggests that both the x and y scales are of order $\delta^{2/3}$ in the breakdown region, with $\bar{\psi}$ of order $\delta^{4/3}$. The region is therefore asymptotically short for $\delta \ll 1$, relative to the length of the jet, and fat compared to the width of the jet.

To examine the flow in the region it is appropriate to introduce the scaled variables

$$\tilde{x} = (x - x_s) \Big/ \left(\frac{\delta^2 \lambda}{a^2}\right)^{1/3} \quad \text{and} \quad \tilde{y} = y \Big/ \left(\frac{\delta^2 \lambda}{a^2}\right)^{1/3} \tag{6.2}$$

along with a scaled streamfunction

$$\tilde{\psi} = \psi \Big/ \left(\frac{\delta^4}{\lambda a^4}\right)^{1/3} \tag{6.3}$$

and corresponding velocity components defined through the equivalent form of (3.2). The factors of a and λ in these expressions are not crucial but they ensure that the problem in terms of the scaled coordinates can be posed in its simplest form. Transforming the equations, the vorticity equation (2.10) reduces to the inviscid form

$$\tilde{u} \frac{\partial \tilde{\zeta}}{\partial \tilde{x}} + \tilde{v} \frac{\partial \tilde{\zeta}}{\partial \tilde{y}} = -\tilde{\zeta} \tag{6.4}$$

for $\delta \ll 1$, where ζ has been scaled to $\tilde{\zeta}$ based on the scales for $\tilde{\psi}$, $\tilde{x}$ and $\tilde{y}$ given above. This is equivalent to the equation solved on the approach to the singularity in Sec. 5, where the flow was also inviscid to leading order, except that now the streamfunction and vorticity are related through the elliptic equation

$$\tilde{\nabla}_h^2 \tilde{\psi} = \tilde{\zeta}\,, \tag{6.5}$$

with the obvious definition for $\tilde{\nabla}_h^2$. It is the presence of the $\tilde{x}$ derivatives in this equation which enables the singularity to be resolved.

The boundary conditions on the flow governed by (6.4) and (6.5) are determined by the inflow of fluid from the erupting jet as $\tilde{x} \to -\infty$, which is a region of thickness in $\tilde{y}$ of order $(-\tilde{x})^{-1/2}$, and by matching to an appropriate potential-flow solution on all other (outflow) boundaries, where $\tilde{x}^2 + \tilde{y}^2 \gg 1$. This latter condition is appropriate since (6.4) implies that the vorticity will decay to zero along all streamlines and therefore that, far from the inflow, $\tilde{\nabla}_h^2 \tilde{\psi}$ will equal zero. More precisely, scaling (5.8) implies that

$$\tilde{\psi} \sim -(-\tilde{x})^{1/2} \tanh[\tilde{y}(-\tilde{x})^{1/2}] \tag{6.6}$$

for $\tilde{y}$ of $O(-\tilde{x})^{-1/2}$ as $\tilde{x} \to -\infty$, while a potential-flow solution which matches (4.6) and tends to a stagnant flow at infinity is

$$\tilde{\psi} \sim -\tilde{r}^{1/2} \sin \frac{\tilde{\theta}}{2} \tag{6.7}$$

for $\tilde{r} \gg 1$, with polar coordinates $(\tilde{r}, \tilde{\theta})$ defined in the usual way. As a result, the streamlines follow the parabolae

$$\tilde{y}^2 = 4\tilde{\psi}^2(\tilde{x} + \tilde{\psi}^2)\,, \tag{6.8}$$

once they have left the jet outflow for $\tilde{y} \gg (-\tilde{x})^{-1/2}$, when $\tilde{x}$ is large and negative.

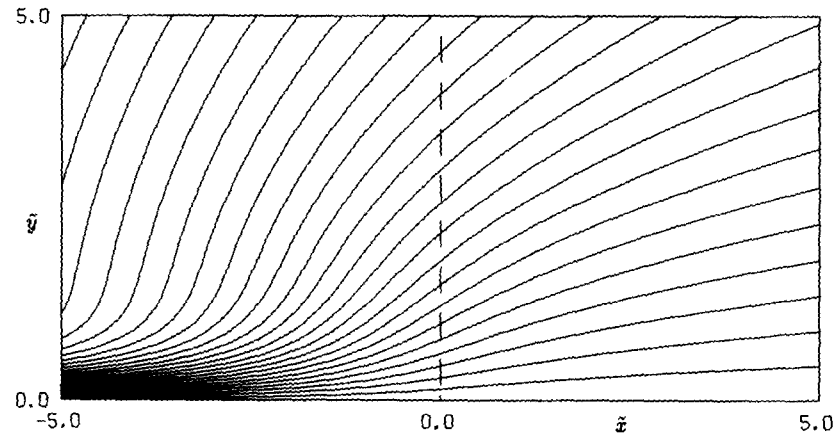

Fig. 7. Streamlines of the scaled streamfunction $\tilde{\psi}$ within the inviscid region at the end of the jet, described in Sec. 6. The flow is plotted over the region $-5 \leq \tilde{x} \leq 5$ and $0 \leq \tilde{y} \leq 5$ with contour interval $\Delta\tilde{\psi} = 0.1$.

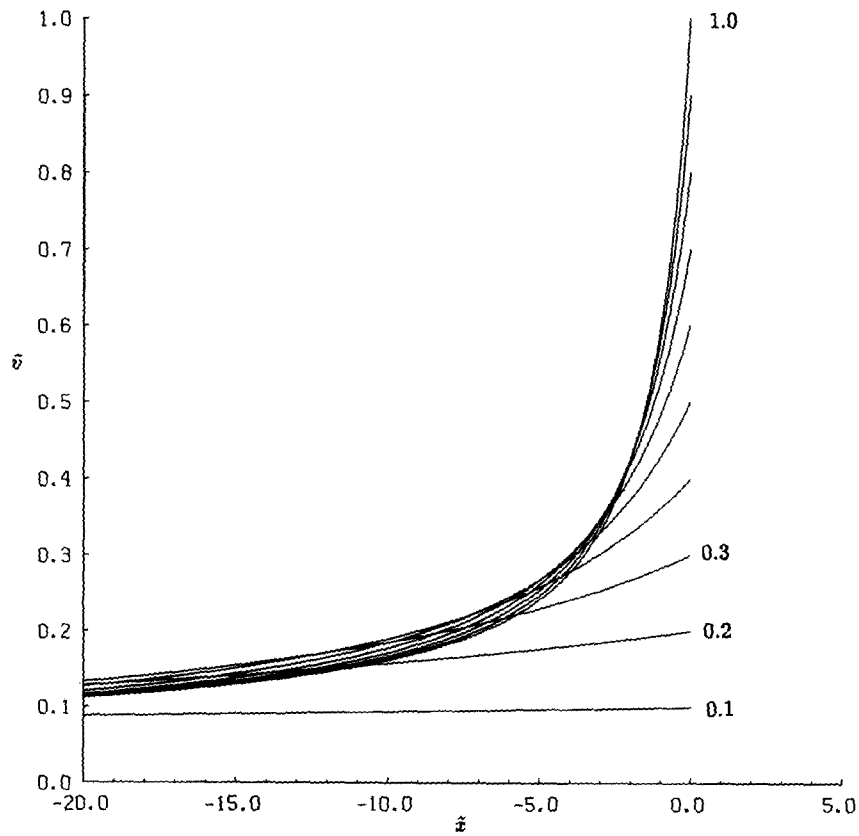

Fig. 8(a).

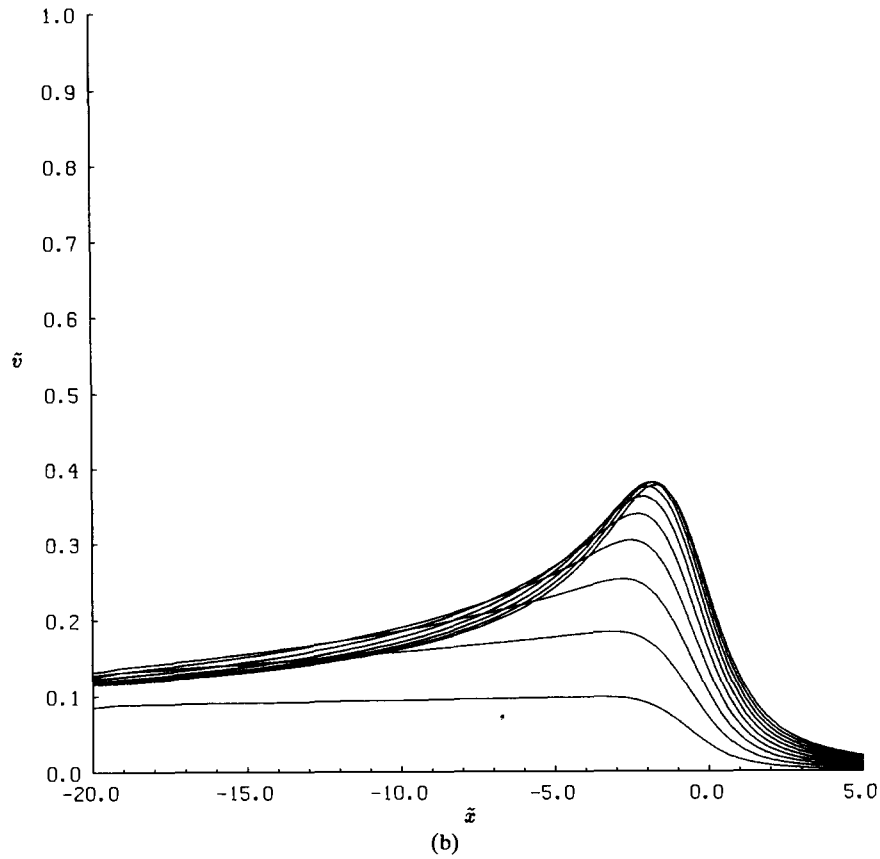

Fig. 8. Cross-sections of the values of the transverse velocity $\tilde{v}$ along various lines $\tilde{y} = constant$ based on (a) the upstream similarity solution (6.6) and (b) numerical solutions of (6.4) and (6.5).

To ensure that the equations (6.4) and (6.5) are able to resolve the singularity, and that matching onto (6.7) is appropriate, the equations were solved numerically in a region with $-20 \leqslant \tilde{x} \leqslant 5$ and $0 \leqslant \tilde{y} \leqslant 5$, with the initial value of $\tilde{\zeta}$ based on the second derivative of (6.6) at $\tilde{x} = -20$ and the boundary conditions for the Poisson equation (6.5) based on a composite form of (6.6) and (6.7). The discretisation of (6.4) was based on similar principles to the box method (Keller and Cebeci [17]), and the solution was obtained by marching in $\tilde{x}$ starting from the initial condition. The Poisson equation (6.5) was discretised using a standard five-point stencil and solved directly using a cyclic-reduction method. Both equations were then solved alternatively using an iterative process until convergence to within a relative accuracy of 0.01% was obtained.

The resulting streamlines for the flow are shown in Fig. 7, and these are markedly different from the corresponding plot in Fig. 6, where no streamlines extend beyond $\bar{x}_s$ (equivalent to $\tilde{x} = 0$). It is apparent that, as the vorticity decays towards the end of the jet, the streamlines match smoothly onto the potential flow (6.7), with velocities gradually tending towards zero, in proportion to $\tilde{r}^{-1/2}$, as $\tilde{r} \to \infty$. Of particular interest is the manner in which the discontinuity in the transverse velocity $\tilde{v}$ is smoothed out, and so cross-sections for this quantity are presented in Fig. 8 for various fixed values of $\tilde{y}$, along with the corresponding behaviour predicted by the similarity solution (6.6). For finite values of $\tilde{y}$, the latter show a jump discontinuity in $\tilde{v}$ at $\tilde{x} = 0$, and from Fig. 8(a) it is clear that the strength

of this increases as $\tilde{y}$ is increased (becoming unbounded as $\tilde{y} \to \infty$). The corresponding solutions of (6.4) and (6.5), shown in Fig. 8(b), match onto the behaviour in Fig. 8(a) for large negative values of $\tilde{x}$ but, as $\tilde{x}$ becomes of O(1), the velocities start to decrease and eventually approach zero as $\tilde{x} \to \infty$. Plots of $\tilde{u}$ and $\tilde{\zeta}$ show similar, but less dramatic, smoothing of the singularity across the region.

7. Induced inviscid flow

As with most boundary-layer flows, the influx and efflux at the outer edge of the jet, as $\bar{y} \to \infty$, induces a larger-scale inviscid flow in the otherwise stagnant fluid surrounding the jet. For a flow with $\bar{c} \ll 1$ this fluid feeds the jet profile for small values $\bar{x}$ and then, once the jet begins to detrain fluid beyond $\bar{x} \approx 0.302$ (see Fig. 2), the small fluid is returned to the exterior of the jet to join a slow recirculation containing velocities of order δ. Within this recirculation region the x and y scales are both of $O(\lambda)$ and so, as a consequence of (2.10), the flow must be irrotational, with the jet appearing as a line source of fluid along the x axis in the $\delta \ll 1$ limit. The flow for $\bar{c} \ll 1$ therefore satisfies the condition $\psi = 0$ both on $x = 0$ and on $y = 0$ for $x > x_s$, where $x_s = \lambda \bar{x}_s$, while at the outer edge of the jet, for $0 < x < x_s$, the values of ψ are $\mp \delta \bar{\psi}_\infty(x/\lambda)$ on $y = \pm 0$.

An exact solution to this potential-flow problem can be derived using standard Green's function methods and it has the form

$$\psi(x, y) = \frac{4xy}{\pi} \int_0^{x_s} \frac{\psi(x', +0)x' \, dx'}{[(x - x')^2 + y^2][(x + x')^2 + y^2]} \tag{7.1}$$

in terms of the values $\psi(x', +0) = -\delta F(x'/\lambda)$ at the edge of the jet. The corresponding streamlines have been plotted in Fig. 9 and these indicate that the influence of the jet extends an $O(\lambda)$ distance from the source through this slow secondary flow. The detail of the flow near the point $(x, y) = (x_s, 0)$ is similar to that shown in Fig. 8, confirming the smooth matching of this flow with that described in Sec. 6. Although a tangential velocity is induced against the wall at $x = 0$ by this secondary flow, the relatively slow speed of the flow in the $E^{1/4}$ layer near $x = 0$ ensures that it acts passively in the parameter range considered here and will not separate. Far from the source, the solution in (7.1) has the form

$$\psi(x, y) \sim C \frac{xy}{(x^2 + y^2)^2} , \tag{7.2}$$

where

$$C = \frac{4}{\pi} \int_0^{x_s} \psi(x', +0)x' \, dx' , \tag{7.3}$$

and this indicates that the corresponding velocities decrease rapidly, in proportion to r^{-3}, as the distance r from the source increases. In fact, using (3.4), it can be shown that C is related to the integral of the momentum flux, through

$$C = -\frac{2}{\pi} \int_0^{x_s} J(x') \, dx' . \tag{7.4}$$

Also apparent in Fig. 10 is that an $O(\delta)$ velocity is induced by the secondary flow on $y = \pm 0$, and this forces an $O(\delta)$ perturbation to the motion in the jet described in Sec. 3. This perturbation is, however, unlikely to change the leading-order flow through any interaction, except perhaps in a very small region near $x = 0$.

For $\bar{c}$ of $O(1)$ the qualitative form of the secondary flow remains similar except that, in addition to the recirculating flow, there is a finite mass flux (of order δ) through the source which produces a corresponding outflow far from the source with

$$\psi \sim \frac{2}{\pi} \delta \bar{\psi}_\infty(0) \arctan(y/x) \tag{7.5}$$

as $r \to \infty$. Using the linearity of the problem, this contribution can be added onto the solution (7.1), with the values of $\psi(x' + 0)$ based on the numerical calculations of $\bar{\psi}_\infty(x/\lambda)$. The resulting velocities far from the source are proportional to r^{-1} in this case, rather than r^{-3} as deduced above for $\bar{c} \ll 1$.

Due to the thinness of the jet relative to its length, for $\delta \ll 1$, the analysis in Secs. 3–6 remains valid for other than semi-infinite regions of fluid, provided there are no obstructions to the jet flow for $0 < x < x_s$. However, the induced flow, such as that shown in Fig. 9, is altered when the inflow is forced by something other than a point momentum source or when the geometry of the stagnant region is different. However, this has no effect on the leading-order properties of the jet.

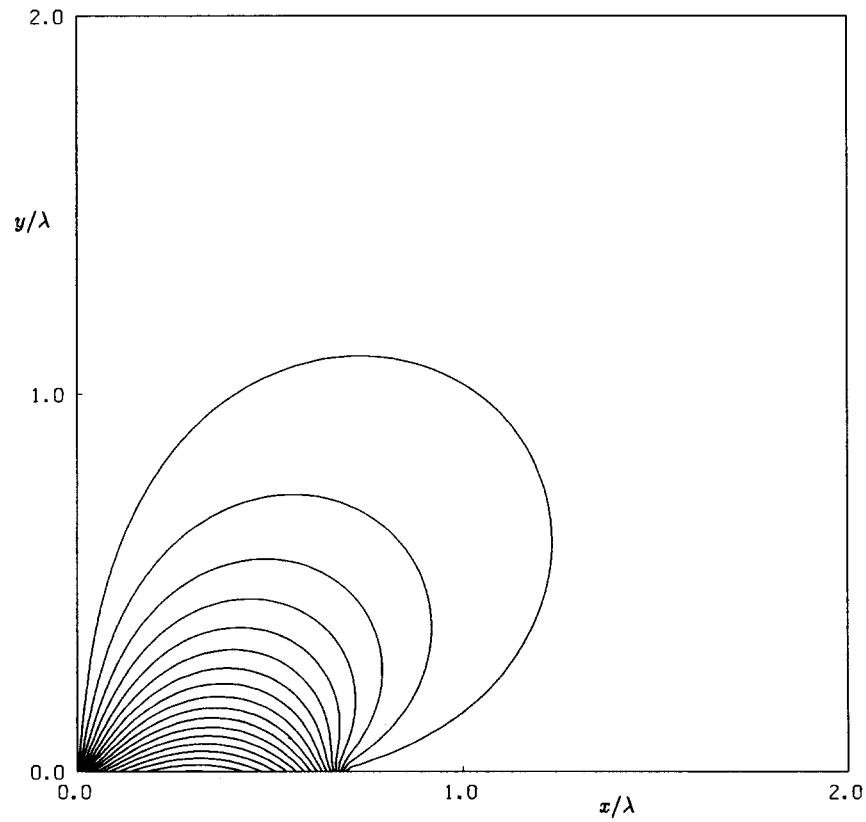

Fig. 9. The $O(\delta)$ streamlines induced by the inflow and outflow from the jet plotted over the region $0 \leq x/\lambda \leq 2$ and $0 \leq y/\lambda \leq 2$, with contour interval $\Delta\psi = 0.05\delta$.

8. The case $\bar{c} \gg 1$

Some of the modifications to the flow in the jet as $\bar{c}$ is increased for a particular form of profile were noted from the plots of the exact solution for a sech^2 profile, shown in Fig. 3. The same exact solution tends to the form (5.9) for $\bar{c} \gg 1$, with the singularity $\bar{x}_s \to (12\bar{c})^{-1/2}$ and a approaching $(3\bar{c}^3/4)^{-1/4}$, and this indicates that the flow becomes effectively inviscid as $\bar{c}$ becomes large. More generally, comparing the sizes of the $\partial^2\bar{u}/\partial\bar{y}^2$ and $\bar{u}$ terms in (2.14) for a general initial profile of the form

$$\bar{u}_0(\bar{y}) = (\bar{c})^{-1/2} U(\bar{y}/\bar{c}) , \tag{8.1}$$

it is clear that the former are relatively small as $\bar{c} \to \infty$ and that the subsequent development of the jet will be governed by (5.1) rather than the full equation.

Solutions of (5.1) for various forms of initial profile were examined by both Gadgil [12] and Moffatt and Toomre [16] in cases where the function h in (5.2) takes a simple form and

$$-\frac{\partial\bar{\psi}}{\partial\bar{y}} = (\bar{x}_s - \bar{x}) - h(\bar{\psi}) \tag{8.2}$$

can be integrated analytically to yield $\bar{\psi}(\bar{x}, \bar{y})$. In all of these cases the solution had a singularity at the point $\bar{x}_s = \bar{u}_0(0)$, of magnitude $\bar{c}^{-1/2}$ for $c \gg 1$ with the normalisation in (2.20), and Gadgil [12] noted that for each of his profiles the flow developed into a similar form to the similarity solution (5.9) as $\bar{x} \to \bar{x}_s$. From the analysis in Sec. 5 it is clear that this

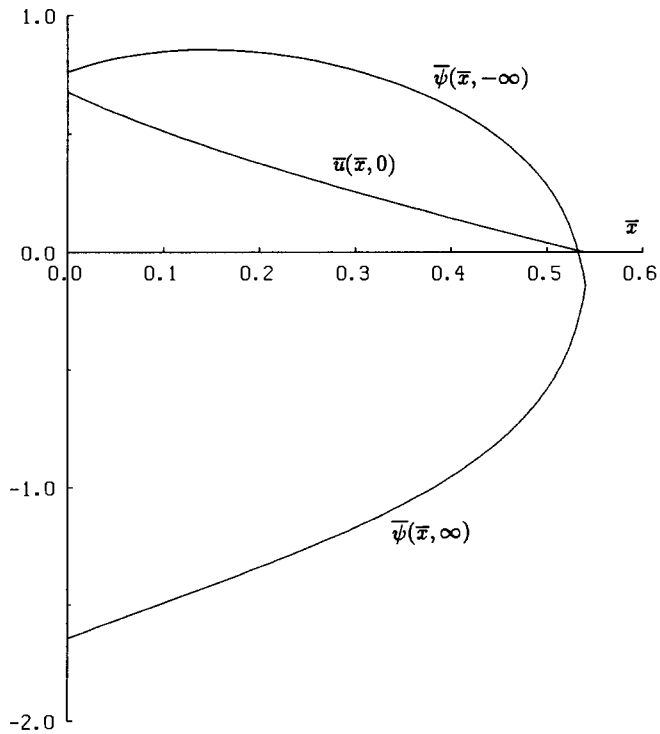

Fig. 10. Plots of $\bar{\psi}(\bar{x}, \pm\infty)$ and $\bar{u}(\bar{x}, 0)$ for the inflow profile (9.2) with $\bar{c} = 1$.

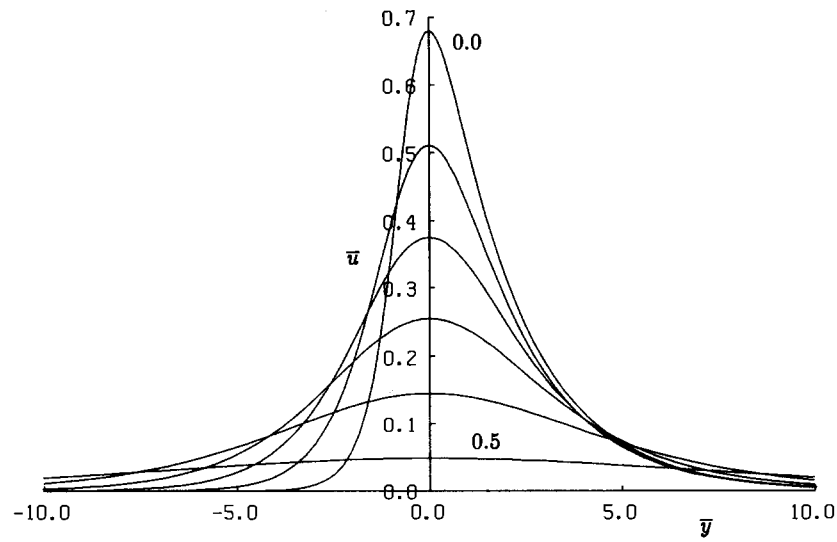

Fig. 11. Plots of the velocity profiles $\bar{u}(\bar{x}, \bar{y})$ based on numerical calculations with the initial profile (9.2) with $\bar{c} = 1$, plotted at $\bar{x} = 0.0, 0.1, 0.2, \ldots, 0.5$.

must occur because, for the profiles chosen by Gadgil, $h(\bar{\psi})$ is proportional to $\bar{\psi}^2$ for $\bar{\psi}$ small and therefore (8.2) can be approximated by (5.4) close to the singularity. In the more general case of symmetric profile with a single velocity maximum, however, h can take any monotonically increasing form, for example $h = -b^2\bar{\psi}^4$, and this would seem to produce a different limiting solution to that described in Sec. 5. A further example of this is the 'top hat' profile considered by Moffatt and Toomre [16] which is interesting in that the resulting motion is essentially stagnation-point flow within the jet with no motion outside; as a result there is a finite rather than an infinite discontinuity in $\bar{v}$ at $\bar{x}_s$. In both of these exceptional cases, however, there will be a $(1/\bar{c}^2)$ perturbation to h, introduced through the diffusive term in (2.14), which would be proportional to $\bar{\psi}^2$ and sufficiently close to $\bar{x}_s$ this would dominate the leading-order behaviour, finally leading to a profile of the form (5.9).

Once the flow is within a distance of order $\bar{c}^{1/2}\delta^{2/3}$ of $\bar{x}_s$, a similar analysis to that described in Sec. 6 can be used to resolve the singularity in the flow. The size of this region increases with $\bar{c}$ while the length of the jet, of $O(\bar{c}^{-1/2})$, decreases and both are of the same size once $\bar{c}$ is of order $\delta^{-2/3}$. At this stage the size of the breakdown region is of magnitude $\delta^{1/3}$ in both x and y and the equations (6.4) and (6.5) describe the motion of the jet from the point of inflow onwards. With the scaling of the momentum flux based on (2.20), the velocities in this region are of order $\delta^{1/3}$, of the same magnitude as the size of the region. The resulting outer flow, equivalent to that described in Sec. 7, is simply of the form (7.2) everywhere.

9. Asymmetric jets

For a jet with an asymmetric inflow profile, but a single velocity maximum, most of the theory described in the previous sections remains appropriate, subject to minor modifications. For example, when $\bar{c} \ll 1$ the flow develops into a symmetric Bickley-type profile over

a distance of $O(\bar{c})$, so that the resulting flow for $\bar{x}$ of O(1) turns out to be symmetric as in Sec. 3.

For $\bar{c}$ of O(1) the jet develops asymmetrically but, using a Prandtl transformation to define $\bar{y} = 0$ at the maximum of the jet, it is found that a singularity similar to that described in Sec. 5 still occurs as the jet loses momentum. In this case, however, the value of $\bar{\psi}$ need not be zero on $\bar{y} = 0$ on the approach to $\bar{x}_s$, and therefore (5.4) would take the alternative form

$$\bar{u} = (\bar{x}_s - \bar{x}) - a^2(\bar{\psi} - \bar{\psi}_s)^2 . \tag{9.1}$$

This leads to a similar sech^2 profile to (5.9), but with (5.8) shifted by an amount $\bar{\psi}_s$. These differences are illustrated in Fig. 10, where the values of $\bar{u}(\bar{x}, 0)$ and $\bar{\psi}(\bar{x}, \pm\infty)$ are plotted based on numerical solutions for a jet with the initial profile

$$\bar{u}_0(\bar{y}) = \alpha/(e^{2\bar{y}/\bar{c}} + 2e^{-\bar{y}/\bar{c}}) . \tag{9.2}$$

In particular, $\bar{\psi}_s$ is close to 0.14 for this flow and one side of the jet has continuously detrained fluid while the other entrains fluid in the initial stages of the motion. The velocity profiles corresponding to this inflow are shown in Fig. 11, and they indicate that the jet soon develops into a symmetric form, with a sech^2 type profile, as would be expected from (9.1). Thus the approach to the singularity turns out to be symmetric, as before, and the results of Sec. 6 can be applied unchanged. The induced flow described in Sec. 7 will, however, be asymmetric with different values of $\bar{\psi}$ on $\bar{y} = \pm 0$ and therefore (7.1) cannot be applied without modification.

For large values of $\bar{c}$, where the flow within the jet is determined by (8.2), the position of the velocity maximum remains at the same value of $\bar{\psi}$ as the jet proceeds, although the flow develops diffeently on either side of the maximum, as for the $\bar{c} = O(1)$ case. On the approach to the singular point, (5.4) remains accurate (provided $h \propto \bar{\psi}^2$ for $\bar{\psi} \ll 1$) and the flow is locally symmetric. Apart from $\bar{\psi}_s$ being equal to zero, the induced outer flow is similar to that described above for $\bar{c} = O(1)$.

10. Conclusions

The most significant result of the calculations in this paper is the demonstration of the development of a singularity within a wide class of free jet flows in a rotating fluid and the ultimate resolution of this singularity, in the manner described in Sec. 5 and Sec. 6. Initially, the results of Gadgil [12] appear to apply only to the particular case of a jet induced by a momentum source, but, as described in Sec. 4, numerical solutions suggest that a similar form of singularity will occur for any form of jet and that a sech^2 velocity profile must develop on the approach to this point.

On the same basis, as described above, it can be expected that a singularity will form for a jet which moves along a non-slip boundary, for example where a solid wall is inserted along the x axis in Fig. 1. In that case it can be expected that there will be an additional viscous layer close to $\bar{y} = 0$ on the approach to the singularity, rather like the viscous layer in Page [18] and Page and Cowley [19].

One particular case where the results of this study can be applied immediately is to the proposal for the structure of separated flow past a cylindrical object in Page [3], where the

lower part of the separated shear layer is assumed to be turned by 180°, forming into a jet along the axis of symmetry, in the manner of Smith [20]. Although this jet would be singular at its initial point, in the sense that its curvature is unlikely to be finite on the line of symmetry, it can be expected that it would undergo the same process as described in this paper, with its centreline velocity decreasing to zero before it reaches the rear of the cylinder. Whether this occurs depends crucially upon the initial momentum flux of the jet and, modelling it with a Bickley-type source of strength $\bar{J}$, it is a simple matter to show that both the length of the jet and its entrained flux are multiplied by a factor of $(\bar{J})^{1/2}$ when $\bar{J} \neq 1$. As a result, the distance before a singularity is encountered in the flow described above would be equal to $\lambda(\bar{J})^{1/2}\bar{x}_s$ which, when the obstacle is a circular cylinder, would be greater than the length of the separated region (see Page [3]) if $\bar{J}$ is larger than about one. Since much of the momentum of the shear layer would be lost by the time the reattachment point is reached, this would be unlikely, although it would need to be verified by more-detailed boundary-layer calculations for the separated shear layer. However, the absence of such a jet in the finite-δ numerical calculations of both Matsuura and Yamagata [8] and Becker [9] does support this view. As a consequence, the portion of the flow marked III_5 in Fig. 6 of Page [3] would not be present for the separated flow past a cylinder, to $O(\delta)$, which considerably simplifies the calculation of the shear-layer region, marked III_2. For bodies with other shapes, such as the aerofoil shown in Page [5], the jet may still contain fluid when the rear of the obstacle is encountered, and so region III_5 could still exist but may not extend all of the way back to the separation point.

The analysis in this paper is scaled appropriately for a jet with a momentum flux J of $O(\delta)$, but the case $\bar{c} \gg 1$ examined in Sec. 8 is also interesting when J is $O(1)$. In this situation the length of the jet is, from above, of order $(J/c)^{1/2}$ when $c \ll 1$, while the size of the region equivalent to that described in Sec. 6 is $O(c)^{1/2}$. These two regions obviously merge once c is $O(1)$, forming a region with size of $O(c)$ in which (6.4) and (6.5) are appropriate. The flow for $r \gg c$ then has the form (7.2).

Acknowledgements

The authors wish to extend thanks to Dr P.W. Duck, who suggested the problem, to Dr S.J. Cowley for helpful discussions on the material in Sec. 6, to Professor D.L. Boyer who pointed out the work of Gadgil and to Professor N. Riley who alerted them to the earlier work by Moreau, and Moffatt and Toomre.

References

1. J.D.A. Walker and K. Stewartson, The flow past a circular cylinder in a rotating frame, *Zeit. angew Math. Phys.* 23 (1972) 745–752.
2. M.A. Page, Flow separation in a rotating annulus with bottom topography, *J. Fluid Mech.* 123 (1982) 303–313.
3. M.A. Page, Separation and free-streamline flows in a rotating fluid at low Rossby number, *J. Fluid Mech.* 179 (1987) 155–177.
4. M.A. Page, The low Rossby number flow of a rotating fluid past a flat plate, *J. Eng. Math.* 17 (1983) 191–202.
5. M.A. Page, The numerical calculation of free-streamline flows in a rotating fluid at low Rossby number. In: G. de Vahl Davis and C.J. Fletcher (eds), *Computational Fluid Dynamics*. North-Holland (1988) pp. 579–588.
6. D.L. Boyer, Flow past a right circular cylinder in a rotating frame, *Trans. ASME D: J. Basic Engng* 92 (1970) 430–436.

7. D.L. Boyer and P.A. Davies, Flow past a cylinder on a beta-plane, *Phil. Trans. R. Soc. Lond. A* 306 (1982) 533–556.
8. T. Matsuura and T. Yamagata, A numerical study of a viscous flow past a circular cylinder of an f-plane, *J. Met. Soc. Japan* 63 (1985) 151–166.
9. A. Becker, The separated flow past a circular cylinder in a rotating frame, in preparation.
10. W. Bickley, The plane jet, *Phil. Mag. Ser. 7* 23 (1937) 727–731.
11. H. Schlichting, *Boundary Layer Theory*, 5th edn., McGraw-Hill (1966).
12. S. Gadgil, Structure of jets in rotating systems, *J. Fluid Mech.* 47 (1985) 417–436.
13. S.B. Savage and R.J. Sobey, Horizontal momentum jets in rotating basins, *J. Fluid Mech.* 71 (1975) 755–768.
14. D.W. Moore, Homogeneous fluids in rotation, Section A: Viscous effects. In: P.H. Roberts and A. Soward (eds), Ro*tating Fluids in Geophysics*. Academic Press (1978) pp. 29–66.
15. R. Moreau, Jet libre plan, laminaire, d'un fluide incompressible en présence d'un champ magnétique transversal, *C. r. hebd. Séanc. Acad. Sci., Paris* 256 (1963) 2294–2298, 4849–4853.
16. H.K. Moffatt and J. Toomre, The annihilation of a two-dimensional jet by a transverse magnetic field, *J. Fluid Mech.* 30 (1967) 65–82.
17. H.B. Keller and T. Cebeci, Accurate numerical methods for boundary-layer flows. In: M. Holt (ed.), *Proc. 2nd Intl Conf. on Numerical Methods in Fluid Dynamics*. Lecture Notes in Physics, Vol. 8, Springer (1972) pp. 92–100.
18. M.A. Page, On the low-Rossby-number flow of a rotating fluid past a circular cylinder, *J. Fluid Mech.* 156 (1985) 205–221.
19. M.A. Page and S.J. Cowley, On the rotating-fluid flow near the rear stagnation point of a circular cylinder, *J. Fluid Mech.* 194 (1988) 79–99.
20. F.T. Smith, A structure for laminar flow past a bluff body at high Reynolds number, *J. Fluid Mech.* 155 (1985) 175–191.